International Journal of Heat and Technology
Vol. 36, No. 1, March, 2018, pp. 344-352
Journal homepage: http://iieta.org/Journals/IJHT

Numerical investigation on the effect of variation of water level on the stability of soil-cement column reinforced waterway side slope

Li'e Yan[1,2,3], Nianping Yi[1,2,3*], Xingui Zhang[1], Shengcai Xu[4]

[1] College of Civil and Architectural Engineering, Guangxi University, Nanning, China
[2] Key Laboratory of Engineering Disaster Prevention and Structural Safety of Chinese Ministry of Education, Nanning, China
[3] Key Laboratory of Disaster Prevention and Mitigation and Engineering Safety of Guangxi, Nanning, China
[4] He Zhou University, He Zhou, China

Corresponding Author Email: ynp0771@163.com

https://doi.org/10.18280/ijht.360146

Received: 17 September 2017
Accepted: 21 November 2017

Keywords:
unsaturated soil, seepage, stability analysis of side slope, strength reduction finite element method.

ABSTRACT

The variation of water level caused by the impoundment of approach channel for navigation and reservoirs flood relief, will lead to a changing of the water level outside the bank slope and the pore water pressure field inside the slope which handicapped the stability of bank slope. In this paper, ABAQUS finite element software considering the stress-seepage coupling was employed to figure out the influence of variation of water level on the stability of cement shear wall reinforced approach channel side slope, in combination with the strength reduction technique. As a result, the key factors affecting the stability of the reinforced side slope include the velocity of change of channel water level, height of the channel water level, the time effect of pore water pressure inside slope and the permeability coefficient of cement-soil reinforced area. In a practical engineering, it is crucial to check the most dangerous working condition, and measures to optimize the cement-soil reinforced slope structure were proposed which can provide a reference for engineering practices.

1. INTRODUCTION

The stability of the side slope of waterway is different from the side slope of general architecture, because it is influenced by a fluctuation of water lever, which often is the main reason of landslide [1, 2, 3].

There are still many problems to be solved in terms of the heterogeneity and the coupling of the mechanical mechanism of the physical field of the side slope, which are still one of the hottest research topics in geotechnical engineering area.

Lane and Griffiths [4, 5] used a strength reduction finite element technique to analyze the stability of side slope in different static levels and under the situation of a sudden drop of water level, but they did not consider the influence of unsaturated seepage, and did not use the transient analysis method which could reflect the time effect. Berilgen [6] adopted Plaxis software which considers the coupling of stress and seepage, and combined the strength reduction technique to calculate the stability of side slope under the working condition of drawdown. However, in his paper, the whole side slope was deemed at the status of saturation, without considering the reinforcement of unsaturated matric suction to the slope stability. Jia et al. [7] analyzed the stability of earth dam under the action of unsaturated unsteady seepage in detail using the strength reduction finite element method, and made a comparison with traditional limit equilibrium method to prove the effectiveness of the strength reduction finite element method, but her research did not study the matrix suction of the unsaturation area. Zhang et al. [8] considers the function of matric suction when analyzing the characteristics of the unsteady seepage field of the unsaturated soil embankments during the fluctuation of river water level. However, she regarded the matric suction as an average constant, which ignores the impact of saturability on matric suction. Nian et al. [9] adopted Abaqus to calculate the strength reduction of the side slope which considers the unsaturated-unstable seepage and studied the overall stability of the bank slope during the drawdown process. However, he did not describe the implementation procedure of the strength reduction method which is used to analyze the side slope stability in consideration of the unsaturation-unsteady seepage effect in Abaqus.

Overall, most of recent researches simplify the treatment of saturation-unsaturation seepage, and seldom consider the influence of stress-seepage coupling and time effect during the variation of water level [10]. The way how to organically combine seepage, deformation and destruction process and authentically reflect the influence of variation of water level on the stability of bank slope is still worth to be further studied [11]. Taking advantage of the powerful stress-seepage coupling analysis function of Abaqus and in combination with the strength reduction technique, this paper studies the stability of the reinforced side slope under the action of stress-seepage coupling, which was a approach channel side slope reinforced with cement soil shear wall, probes into the influence rule of reinforced side slope seepage field and stability under the fluctuation of water level and puts forward relevant suggestions for design and construction.

2. THEORY OF SATURATED-UNSATURATED SOIL SEEPAGE CONSOLIDATION

2.1 Seepage of saturated-unsaturated soil and its strength characteristics

In the liquid seepage flow-stress coupling analysis, the permeability coefficient of soil must be defined, and Forchheimer law was adopted by Abaqus as the permeability law [12]. As the permeability coefficient of unsaturated soil is relevant to the matrix suction which is hard to be measured, it is hard to conduct the experiment for obtaining the soil-water characteristic curve. The classical Van Genuchten model was employed in this paper to make the analysis easier [13]. Its permeability coefficient model, soil-water characteristic curve model and the expression of its derivative form are as follows:

$$S_e = (S - S_r)/(1 - S_r) = [1 + (\alpha\Phi)^n]^{-m} \tag{1}$$

$$C_S = \partial S/\partial \Phi = \alpha(1-n)(1-S_r)S_e^{1/m}(1-S_e^{1/m})^m \tag{2}$$

$$k = k_s k_r = k_s S_e^{1/2}[1-(1-S_e^{1/m})^m]^2 \tag{3}$$

where, S, S_r, and S_e are the saturation degree, residual saturation and effective saturation degree, respectively; Φ is the matrix suction; k_s is the saturation permeability coefficient; k_r is the relative permeability coefficient of unsaturated soil; α, m and n are the fitting parameters of soil-water characteristic curve, in which $m = 1 - 1/n$.

In unsaturated soil, the Terzaghi principle of effective stress cannot be used directly because of the impact of matrix suction, so that the improved principle of effective stress of the unsaturated soil proposed by Bishop in 1959 was employed in this article.

2.2 Governing equation of stress-transfusion coupling

2.2.1 Stress equilibrium equation

The saturated-unsaturated soil was assumed to be a continuous medium. Based on the variational principle of potential energy of continuous medium, the differential equation of stress equilibrium and stress boundary condition can be translated into an equivalent integral form (i.e. virtual work equation). Take a derivative of time in the virtual work equation, i.e. making analysis of the coupling of stress and seepage. Therefore, the equivalent integral form of stress equilibrium equation of saturated-unsaturated soil is as below:

$$\begin{aligned}&\int_V \delta\varepsilon^{\mathrm{T}} D_{\mathbf{ep}} \frac{\partial\varepsilon}{\partial t}\mathrm{d}V - \int_V \delta\varepsilon^{\mathrm{T}} m(s + C_s u_w)\frac{\partial u_w}{\partial t}\mathrm{d}V = \\ &\int_V \delta u^{\mathrm{T}} \frac{\partial f}{\partial t}\mathrm{d}V + \int_S \delta u^{\mathrm{T}} \frac{\partial p}{\partial t}\mathrm{d}S\end{aligned} \tag{4}$$

where, σ is total stress; $\delta\varepsilon$ and δu are virtual strain and virtual displacement, respectively; f is unit volume force, and it is the sum of the weight of the soil skeleton and the weight of water for unsaturated soil; p is boundary surface force; m = [1, 1, 1, 0, 0, 0]$^{\mathrm{T}}$; S is saturability; C_s is the rate of change of the saturability of the unsaturated soil relative to matrix suction, which can be calculated according to a soil-water characteristic curve.

2.2.2 Seepage continuity equation

With the assumption of incompressible soil particles and water, an infinitesimal volume of soil was studied based on the principle of mass conservation. The amount of water streaming in and out of the micro-body within the period of d_t equals to the quality change of the micro-body, and the seepage of liquid can be described according to Darcy law. The tension strain was set as positive. The seepage continuity equation of saturated-unsaturated soil was obtained from derivation. The pore pressure boundary conditions were introduced into the finite element equation as a coercive boundary condition, thus the discharge boundary condition and seepage continuity equation can be translated to an equivalent integral form:

$$\begin{aligned}&\int_V \nabla(\delta u_w) k \nabla\left(\frac{u_w}{\gamma_w} + z\right)\mathrm{d}V + \int_S \delta u_w q\,\mathrm{d}S + \\ &\int_V \delta u_w \left(s\frac{\partial\varepsilon_v}{\partial t} + nC_s\frac{\partial u_w}{\partial t}\right)\mathrm{d}V = 0\end{aligned} \tag{5}$$

where, ∇ is hamiltonian operator; δu_w is the variation of pore pressure function; ε_v is volumetric strain; n is porosity; u_w is pore water pressure; q is water discharge going through the boundary in unit time, and when it has a same direction with n, it is positive.

3. FINITE ELEMENT STRENGTH REDUCTION TECHNIQUE UNDER THE INFLUENCE OF STRESS-SEEPAGE COUPLING

Abaqus can be employed to estimate and analyze plane strain, axial symmetry and coupling of 3D fluid seepage-stress. Thereinto, finite element strength reduction method showed a good application effect in the analysis of the stability of side slope [14, 15]. In this method, according to Equation, the soil strength of side slope was reduced. If the side slope stayed at a stable state, the reduction coefficient shall be continuously increased until an appearance of buckling failure in the side slope, and the reduction coefficient F_{sr} of this time was defined as the security coefficient of side slope stability.

$$c_m = \frac{c}{F_{sr}}, \quad \varphi_m = \arctan\left(\frac{\tan\varphi}{F_{sr}}\right) \tag{6}$$

where, c and φ are parameter values of shear strength of soil; c_m and φ_m are parameter values of shear strength of soil at the state of limit equilibrium; F_{sr} is strength reduction factor.

However, researchers had different opinions on the estimation of the critical state of slope instability [16, 17]. The most popular evaluation criterions are as follows: whether the displacement of the feature parts (e.g. slope crest or slope toe) of the side slope mutates, whether successive

penetration area is formed in the side slope and whether the numerical calculation converge. Combining with the engineering projects, the misconvergence of numerical computation and sharp increase of joint displacement at feature parts were used as the instability criterion in this paper.

Liquid-solid coupling process and the analysis method of finite element strength reduction separation were used to solve the problem of overcomputation of finite element numerical value and convergence difficulties [18, 19], i.e. first figure out the seepage field of the side slope at different times using the saturation-unsaturation liquid-solid coupling finite element procedure, and then translate the fluid gravity and pore pressure of the seepage field into equivalent nodal load, which will be imposed to the element node. Finally, the security coefficient of the side slope at any time is analyzed with strength reduction method of single phase solid medium.

4. NUMERICAL CALCULATION MODEL AND RELATIVE PARAMETERS

Previous researches [20] carried out experimental verification using numerical simulation and the horizontal shear model of the pile-soil compound structure. It is believed that it is a fairly sound choice for the side slope governance to connect the pile body into the reinforced structure of cement-soil shear wall as shown in Figure 1 when the cement soil reinforced side slope is adopted. The results show that the cement soil shear wall reinforced side slope can be replaced by an equivalent entity structure as shown in Figure 2 to simplify a 3D problem to a 2D plane problem [21]. On the basis of this study, a stability numerical investigation on the equivalent entity of reinforced side slope under the variation of water level was further studied.

The sources of side slope in this paper were the side slope of downstream approach channel of Line No. 3 and No. 4 navigation locks at Changzhou hydro-junctions, whose gradient was 1:2.5, and their strata include plain fill, clay, silty clay, completely decomposed granite. The most dangerous side slope of downstream approach channel was selected and reinforced with cement-soil shear wall, as shown in Figure 3. The foundation bed surface of the channel was regarded as the water level elevation. H_w , H_S and ΔH are the water level of channel, the water level of far field boundary inside side slope and the difference between the water level inside and outside the slope, respectively. The equivalent entity part in Figure 3 is the 2D simplified cement shear wall reinforced area, whose permeability coefficient was the concentrated expression of the cement-soil permeability coefficient and soil permeability coefficient, which can be acquired according to the equivalent permeability coefficient computational formula of multilayered subgrade at the situation of horizontal seepage [22].The parameters of the soil layer of the side slope and the equivalent of each soil layer can be seen in Table 1 and Table 2. The material parameters related to seepage were shown in Table 3.

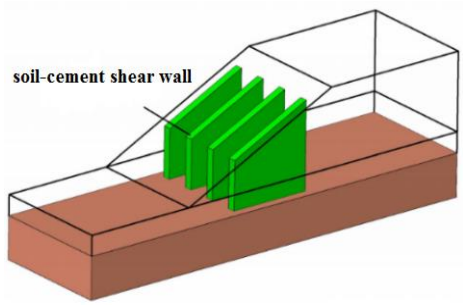

Figure 1. The diagram of soil-cement shear wall reinforced slope

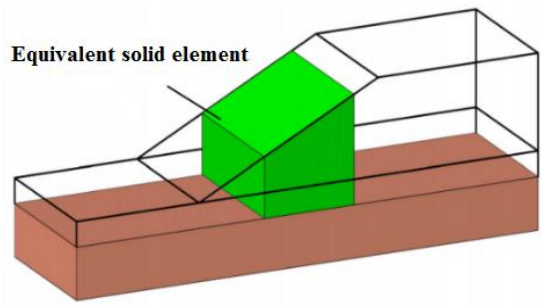

Figure 2. Equivalent entity model of the reinforced slope

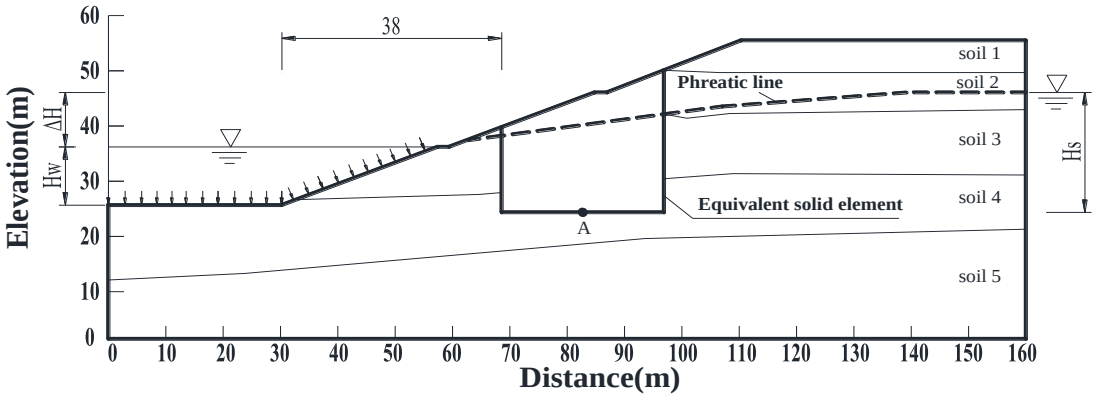

Figure 3. Numerical calculation model of reinforced slope of approach channel in downstream

Table 1. Physico-mechanical parameters of slope soil

Soil Layer Number	Name of Soil Layer	Weight $\gamma\ (KN/m^3)$	Water Content $w(\%)$	Specific Gravity G_s	Modulus of Deformation $E(MP_a)$	Poisson's Ratio υ	Cohesion $c(KP_a)$	Angle of Internal Friction $\varphi(^0)$
	Plain Fill	19.5	24.8	2.70	10	0.36	10	17
2	Taupe Gray Clay	19.4	29.2	2.70	10	0.40	32	11
3	Dark Grey Silty Clay	19.9	26.2	2.70	10	0.40	22	10
4	Completely Decomposed Granite	19.0	18.6	2.74	50	0.30	25	24
5	Strongly Decomposed Granite	25.0	3.2	2.72	100	0.30	300	25

Table 2. Physico-mechanical parameters of soil-cement with respect to soil layers

Number	Material name	Weight $\gamma\ (KN/m^3)$	Modulus of Deformation $E(MP_a)$	Poisson's Ratio υ	Cohesion $c(KP_a)$	Frictional Angle $\beta(^0)$	Tensile Strength $p_t(KP_a)$
1	Soil Layer 1 Equivalent Entity	20	60	0.35	151.17	31.50	120
2	Soil Layer 2 Equivalent Entity	20	60	0.35	181.20	26.68	180
3	Soil Layer 3 Equivalent Entity	20	60	0.35	170.36	25.81	170
4	Soil Layer 4 Equivalent Entity	20	100	0.30	160.87	36.39	100

Table 3. Calculating parameters of soil layers for stress-seepage coupling analysis

Number	Name	Dry Density γ (kg/m^3)	Initial Void Ratio e_0 (%)	Initial Saturability S_r (%)	Saturation Osmotic Coefficient k_s (m/d)	Gravitational Acceleration g (m/s^2)
1	Plain Fill	1563	0.73	100	2.16×10-2	10
2	Taupe Gray Clay	1500	0.80	100	1.14×10-2	10
3	Dark Grey Silty Clay	1577	0.71	100	1.08×10-2	10
4	Completely Decomposed Granite	1602	0.71	100	2.59×10+0	10
5	Strongly Decomposed Granite	2422	0.123	100	3.97×10-1	10
6	Cement Soil	1590	0.700	100	1.04×10-4	10

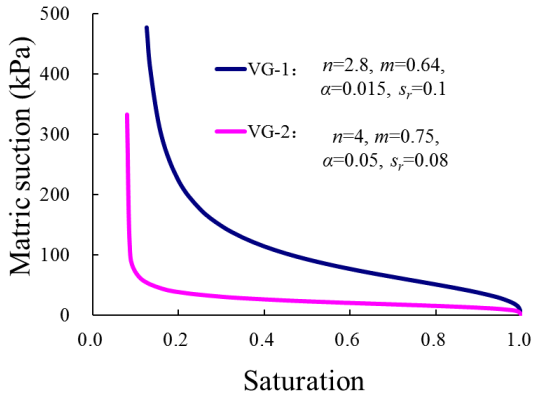

Figure 4. Model of soil-water characteristic curve

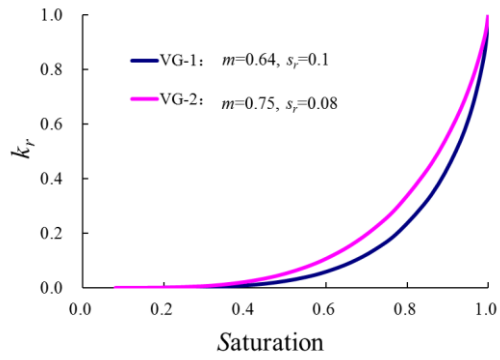

Figure 5. Model of permeability coefficient

The soil-water characteristic curve and osmotic coefficient model of each soil layer used Van Genuchten model, in which the plain fill and clay were VG-1, while granite was respect to VG-2. The VG models of cement soil in each soil layer were assumed to be the same as the VG model of corresponding soil layers. Parameters of VG model were picked out from existing empirical data according to the characteristics of soil layers [23], and the effect of stagnant water was not considered. The finally acquired soil-water characteristic curve model and osmotic coefficient model were shown in Figure 4 and Figure 5, respectively.

5. ANALYSIS OF CALCULATING RESULTS

5.1 The influence of steady seepage on the stability of reinforced side slope

When a water level dropped from a certain attitude and the dropping lasts for a long time, if the waterhead of the far field boundary of the side slope was steady, a steady seepage field will form inside the slope. The effect of water level difference and permeability coefficients in reinforced area on the steady of reinforced side slope was analyzed.

A analysis model was established as below: set up a steady water head boundary at the right boundary of the side slope, H_s = 20 m; lower the water levels of channel with an interval of 2 m, and the variation range of formed water head was 0 ~20 m; two kinds of permeability modes under two limit cases were established according to a possible variation range of osmotic coefficients of the cement-soil reinforced area: ① the permeability coefficient of reinforced area of the slope equals to the model K-1 of the permeability coefficient of the original corresponding soil level, ② the permeability coefficient of reinforced area was the same as the model K-2 of the permeability coefficients of the cement-soil.

Figure 6 showed different waterheads and the corresponding pore-pressure distributions in these two models. In the model K-1, the equivalent permeability coefficients of the reinforced area of the side slope were similar to that of the surrounding soil layers, phreatic line showed a linear decrease trend from right to left, and the egress points were located above the channel's water level, indicating that there still was a water seepage phenomenon at the surface of side slope which was above the channel's water level. In the model K-2, the permeability coefficients in the reinforced area of the side slope were low, which played a role of water proof curtain for seepage, and the intersection point of phreatic line and the right boundary of the reinforced area were obviously higher than these in model K-1, showing the occurrence of water storage effect. When the seepage enters the reinforced areas, the incidence angle of seepage changed, and a large hydraulic slope formed in this area, so that a large seepage force occurred to the reinforced body which was not good for the steady of the side slope.

As seen in Figure 7, with the increase of waterhead and under the effect of seepage force, the glide plane, which appeared when the reinforced side slope was unstable, developed from a superficial layer to a deep layer, and the reinforced side slope showed a significant shear failure model. The bigger the waterhead is, the bigger the seepage force is. Meanwhile, the intensity of the unsaturated soil layer above the phreatic line also increased somewhat. The combined action of the two caused a variation of the security coefficients, as shown in Figure 8. As seen from the graph, when ΔH < 10 m, the negative influences of the increasing water head on the steadiness of side slope outweight the positive influences, and the security coefficients enhanced with the reduction of water head; when ΔH > 10 m, the influences of water head on the steadiness of side slopes were totally different from the former ones. Furthermore, it can also be seen from the figure that the permeability of the reinforced area also influences the transformation law of the stability of side slope, appearing as a lower security coefficient at low permeability condition than the figure at a high permeability condition. The decrease of security coefficient was mainly caused by an increase of the sliding force depending on a larger hydraulic slope formed by the seepage at a low permeability condition.

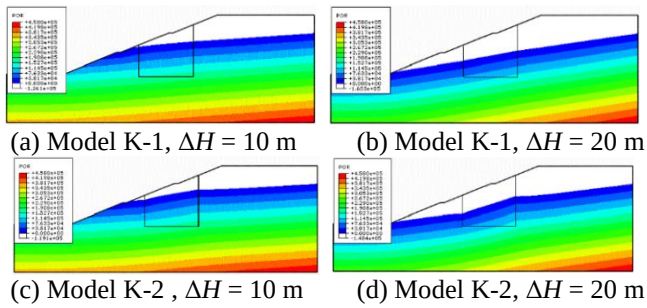

(a) Model K-1, ΔH = 10 m (b) Model K-1, ΔH = 20 m

(c) Model K-2 , ΔH = 10 m (d) Model K-2, ΔH = 20 m

Figure 6. Effect of seepage waterhead on the pore pressure of reinforced slope

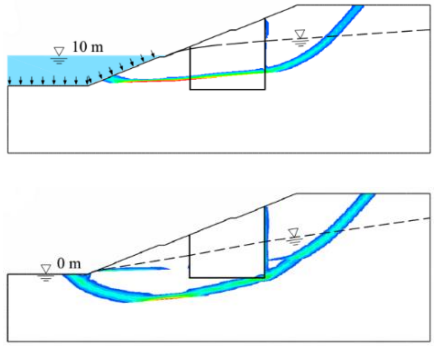

Figure 7. Effect of seepage water head difference on gliding plane

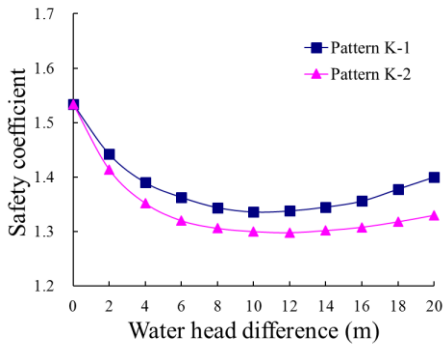

Figure 8. Relation curves of seepage water head difference and safety coefficient

5.2 The influence of rapid drawdown of water level on the stability of reinforced side slope

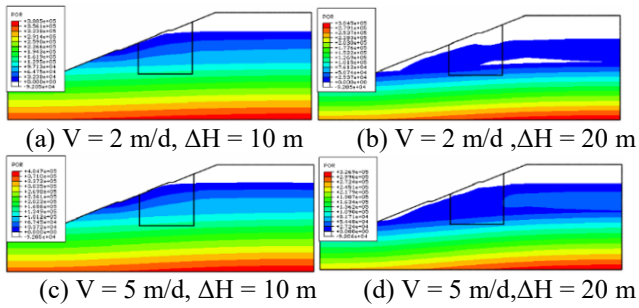

(a) V = 2 m/d, ΔH = 10 m (b) V = 2 m/d ,ΔH = 20 m

(c) V = 5 m/d, ΔH = 10 m (d) V = 5 m/d,ΔH = 20 m

Figure 9. Effect of drawdown speed of water level on pore pressure in the reinforced slope

Figure 9 showed the influence of the suddenly decreased altitude difference and plummeting speed of water level on the pore-pressure field of the reinforced side slope. After a sharp drawdown of water level in a channel, the location variation of phreatic line in the slope obviously lagged behind the variation of the water level of channel. Before the water level drops to the location of completely decomposed granite, the pore water in the side slope mainly permeates from the surface of the side slope which was adjacent to air. As the permeability coefficient is small, the pore pressure inside the side slope did not evanish greatly. However, when the water level drops to the bottom, the underground water inside the slope concentrically drain to the channel via the completely decomposed granite, the pore pressure inside the slope showed a rapid decrease which lead to a small remaining pore pressure as the water level plunge finished. Considering the difference between the seepage force of the clay layers and the granite layers inside the slope, a hollow phenomenon appeared inside the saturated area of the side slope during the process of seepage, so that the pore water at the saturated area which was located above the cavity became the perched water. Besides, the faster the dropdown is, the more obvious the hysteresis effect of the seepage line variation is. Thus, during the water level dropdown process, excess pore water pressure inside the slope cannot be dissipated in time, causing a higher waterhead difference between inside and outside of the slope, which was not good for the stability of the slope.

According to a failure mode of the sliding surface in Figure 10, when a water level sharply decreases, shear failure along with the shear wall and the arc shear sliding failure crossing the completely decomposed granite at the wall base occurred at the reinforced side slope of the approach channel. Slope instability always appeared along the sliding plane which had a smallest sliding resistance force, and changed with the variation of the attitude of water level without any regulations.

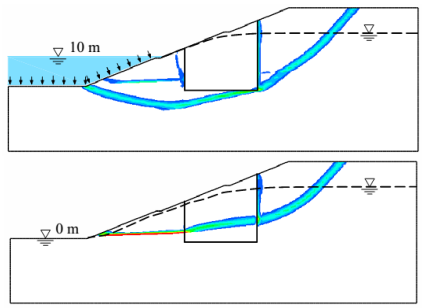

Figure 10. Effect of drawdown on sliding surfaces

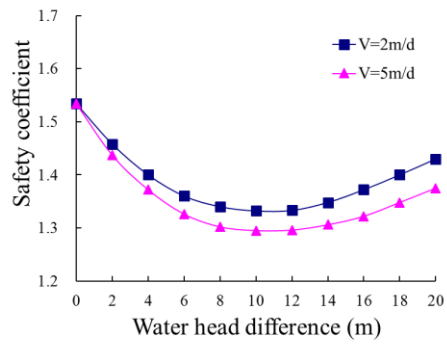

Figure 11. Relation curves of waterhead and security coefficient

As seen from the relation curve of security coefficient of the reinforced side slope and the plunging waterhead in Figure 11, the security coefficient decreased and then increased with the variation of the waterhead, indicating if the plunging waterhead was small, the excess pore water pressure remained in the slope was hard to be dispersed, which reduced the stability of the side slope, but if there is a high plunging waterhead, the pore water inside the slope mainly drained to the channel via the completely decomposed granite, so that the pore pressure inside the slope evanishes quickly, which in turn improved the security coefficient of the side slope. At the same time, the security coefficient decreased with an increasing of the plunging speed, and with the increasing of waterhead, the security coefficient showed a more significant decrease.

Figure 12 showed the flow velocity vector distribution of reinforced side slope in two models, when the water level decreased from 20 m to 6m at the speed of 2 m/d. As seen from the figures, after a plunge of water level, the pore water in the slope flowed downward and concentrically drained into the channel through completed decomposed granite. However, in the K-2 model, as the reinforced area of the side slope had a relatively small permeability coefficient, which hinders the seepage path, the dissipation pf pore pressure slowed down.

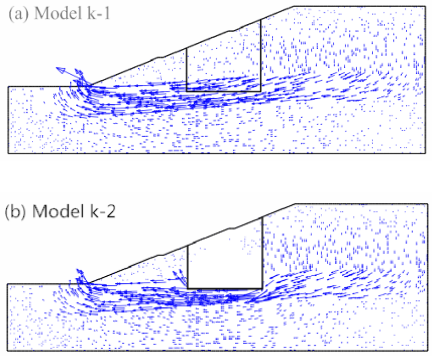

Figure 12. Flow velocity distribution of reinforced slope

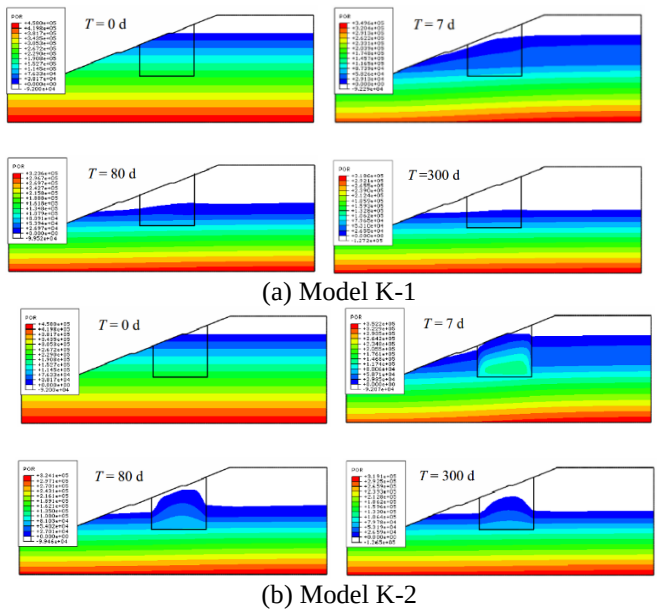

Figure 13. Variation of seepage line in reinforced slope after drawdown of water level

Figure 13 showed a changing process of the phreatic line in slope. As seen from Figure 13 (a), after the water level dropped to the predetermined altitude in 7 days, the location of the phreatic line obviously lag behind the water level of the channel, so there was a larger excess pore water pressure remaining in the slope. The pressure gradually dissipated with the extension of time, and the phreatic line continually dropped down until reaching to the same attitude of the channel water level. In Figure 13 (b), the location hysteresis effect of the phreatic line in the side slope is more obvious than that in model K-1. The differences mainly focused in the reinforced area, indicating that since the permeability of cement is weak, the pore water pressure inside the side slope needs more time to dissipate, and the dropping speed of phreatic line was much slower.

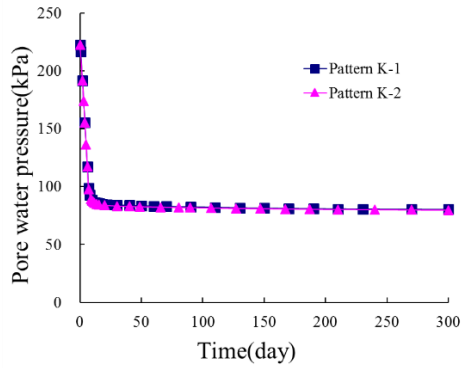

Figure 14. Time-history curves of pore pressure of monitoring point A

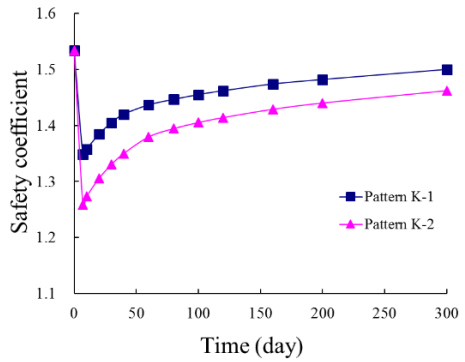

Figure 15. Time-history curves of security coefficient after drawdown of water level

Figure 14 is the time-history curve of pore pressure change of monitoring point A (as seen in Figure 3) during the process of water level plunge, in which the pore pressure at point A sharply decreased at the initial stage of plunge (7 days). The pore pressure continued to dissipate after the stop of plunge, but the speed obviously slows down, and the curve is closed to horizontal.

Figure 15 is the time-history curve of security coefficient of the side slope at the time of water level plunging. The curve development trends of the two models were consistent. At the earlier stage of water level plunging, the security coefficient of the side slope showed a significant decrease, but with the extension of time and the gradually dissipation of pore pressure inside the slope, the security coefficient of the side slope gradually increased, and equaled to the security coefficient for the static level as time approaches infinity. Thus, the side slope was dangerous at the earlier stage of water level plunging, and the stability increased somewhat at the later stage, so that the security coefficient of earlier stage should be considered as the checking point in the practical engineering. Compared with Figure 15, in K-2 model, the security coefficient of reinforced side slope showed a slow recovery speed with the extension of time, and it was always lower than the figures for K-1 model, so that it needed more time to dissipate pore water pressure in the side slope.

5.3 Measures for improving the reinforced structure of the side slope

Through the comparison and analysis of the stability of the reinforced side slope at the working conditions of steady seepage and water level plunging, one can find out that the security coefficients of the reinforced side slope under K-2 model were always lower than those under K-1 model. Therefore, the water stop phenomenon should be avoided when designing and constructing the soil-cement column reinforced waterway side slope. If a soil cement shear wall was connected by cross wall to form a grilling reinforced structure, as seen in Figure 16 (a), in spite of the increase of the integral rigidity of the structure, its water stop effect decreased the stability of the reinforced side slope. If the reinforce structure formation showed in Figure 16 (b) was used, i.e. a suitable seepage path was set at intervals in the grid structure to eliminate a water stop effect of reinforced area, thus further improving the stability of reinforced side slope.

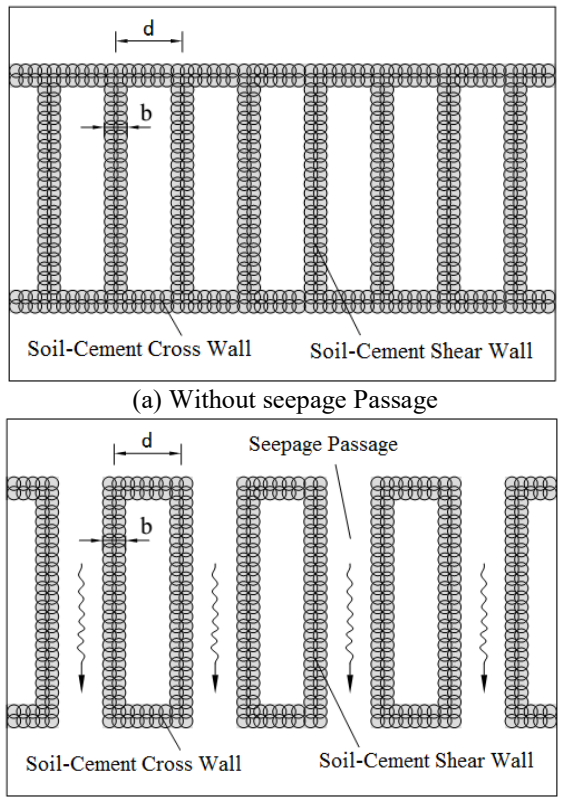

Figure 16. The soil-cement grilling structure of reinforced approach channel slope

6. CONCLUSIONS

A variation of the water level is known as one of the most important factors of the failure of channel side slope. In this paper, The ABAQUS finite element software considering the stress-seepage coupling action was employed to figure out the influence of steady seepage and water level plunging working conditions on the stability of reinforced side slope in combination with the strength reduction technique. The conclusions are as followings:

1) Research at the working condition of steady seepage show that with an increase of waterhead, the glide plane, which appeared when the reinforced side slope was unstable, developed from a superficial layer to a deep layer, and the reinforced side slope showed a significant shear failure model; the smaller the permeability of the reinforced area of the side slope is, the smaller the security coefficient of the side slope is.

2) When the water level plunges, the security coefficient increased at first and then decreased. At the earlier stage of water level plunging, the security coefficient of the side slope showed a significant decrease, but with the extension of time, the security coefficient of side slope gradually increased. The security coefficient of earlier stage shall be considered as a checking point in the practical engineering. At the same time, the faster the drawdown is, the smaller the side slope security coefficient is. In addition, with the increase of the water head, the security coefficient lowers down apparently.

3) Measures for improving the soil cement reinforced side slope structure was proposed: connecting the soil cement shear walls with cross walls to form a grilling reinforced structure and intervally setting a suitable seepage path in the grid structure to further improve the stability of the reinforced side slope.

ACKNOWLEDGMENT

Projects of National Natural Science Foundation of China (NSFC) (51168005, 51268003); Open Program of Guangxi Prevention and Reduction of Natural Disasters and Engineering Safety Key Laboratory (2012ZDK08, 2015ZDK001); Systematic Research Projects of Guangxi Key Laboratory (2013ZDX11); Excellent Doctoral Candidate's Going Abroad Program of Guangxi University; Scientific Research and Technological Development Plan of Nanning (Scientific Key Project), NKFZ No. [2013] 46.

REFERENCES

[1] Chen H. (2016). Analysis of numerical simulation of wading landslide in Three Gorges Reservoir area based on outang landslide. Mathematical Modelling of Engineering Problems 3(2): 71-74. https://doi.org/10.18280/mmep.030205

[2] Guerra AJT, Fullen MA, Jorge MDCO, Bezerra JFR, Shokr MS. (2017). Slope processes, mass movement and soil erosion: a review. Pedosphere 27(1): 27-41.

[3] Chen H. (2016). Analysis of numerical simulation of wading landslide in Three Gorges Reservoir area based on Outang Landslide. Mathematical Modelling of Engineering Problems 3(2): 71-74. https://doi.org/10.18280/mmep.030205

[4] Grifffiths DV, Lane PA. (1999). Slope stability analysis by finite elements. Geotechnique 49(3): 387-403. https://doi.org/10.1680/geot.51.7.653.51390.

[5] Lane PA, Griffiths DV. (2000). Assessment of stability of slopes under drawdown conditions. Journal of Geotechnical and Geoenvironmental Engineering 126(5): 443-450. https://doi.org/10.1061/ (ASCE)1090-0241 (2000)126:5 (443).

[6] Berilgen MM. (2007). Investigation of stability of slopes under drawdown conditions. Computers and Geotechnics 34(2): 81-91. https://doi.org/10.1016/j.compgeo.2006.10.004.

[7] Jia CQ, Huang MS, Wang GH. (2007). Strength reduction FEM in stability analysis of soil slopes subjected to transient unsaturated seepage. Chinese Journal of Rock Mechanics and Engineering 26(6): 1290-1296.

[8] Zhang FZ, Chen XP. (2011) .On seepage flow and stability of unsaturated soil embankment. Rock and Soil Mechanics 32(5): 1561-1567.

[9] Nian TK, Wan SS, Jiang JC, Luan MT. (2010). Finite element analysis of slope stability under drawdown conditions by strength reduction technique. Rock and Soil Mechanics 31(7): 2264-2269.

[10] Vlad D, Coldea AM, Iridon AML. (2016).Study on the water vapor permeability through geotextiles used in repair/stabilizing roads. Academic Journal of Manufacturing Engineering 14(2): 102-106.

[11] Wang GJ, Yang S, Kong XY, Tang YJ. (2016). Study on the process and mechanism of indoor overtopping dam-failure of tailings dam model experiment under the rainfall. Modelling, Measurement and Control C 77(1): 86-97.

[12] Weber L, Ingram D, Guardia S, Athanasiou-Ioannou A, Mortensen A. (2016). Fluid flow through replicated microcellular materials in the darcy-forchheimer regime. Acta Materialia 126: 280-293. https://doi.org/10.1016/j.actamat.2016.12.067.

[13] Song YS, Chae BG, Lee J. (2016). A method for evaluating the stability of an unsaturated slope in natural terrain during rainfall. Engineering Geology 210: 84-92.https://doi.org/10.1016/j.enggeo.2016.06.007.

[14] Li J, Yan S, Zhou YH, Yang KX. (2015). Simulations and comparisons of D-section cylinder in the different Re flow. Mathematical Modelling of Engineering Problems 2(4): 23-28. https://doi.org/10.18280/mmep.020405.

[15] Tschuchnigg F, Schweiger HF, Sloan SW. (2015). Slope stability analysis by means of finite element limit analysis and finite element strength reduction techniques. Part ii: back analyses of a case history. Computers & Geotechnics 70: 178-189. https://doi.org/10.1016/j.compgeo.2015.07.019.

[16] Pei LJ, Qu BN, Qian SG. (2010). Uniformity of slope instability criteria of strength reduction with FEM. Rock and Soil Mechanics 31(10): 3337-3341.

[17] Smith JV. (2015). A new approach to kinematic analysis of stress-induced structural slope instability. Engineering Geology 187: 56-59. https://doi.org/10.1016/j.enggeo.2014.12.015.

[18] Chen H. (2016). Analysis of numerical simulation of wading landslide in Three Gorges Reservoir area based

on Outang Landslide. Mathematical Modelling of Engineering Problems 3(2): 71-74. https://doi.org/10.18280/mmep.030205
[19] Xia J, Xiao L, Wan LP. (2016). Application of random-fuzzy probability statistics method. Mathematical Modelling of Engineering Problems 3(1): 19-24. https://doi.org/10.18280/mmep.030103
[20] Xu SC, Zhang XG, Ma FR, Chen ZX. (2017). Analysis of failure behaviour of slope reinforced by soil-cement column and model test. Rock and Soil Mechanics 11: 1-10. https://doi.org/10.16285/j.rsm.2017.11.014.
[21] Liu WP, Luo XY. (2016). Elastoplastic analysis of circular tunnel using nonlinear improvement of unified strength theory. Modelling, Measurement and Control B 85(1): 163-174.
[22] Wang TZ, Wang CM, Huang XH, Zhu HB. (2016). Spatial distribution of accumulation landslide thrust based on transfer coefficient method. International Journal of Heat and Technology 34(2): 287-292. https://doi.org/10.18280/ijht.340219
[23] Lorenzini G, Lara MFE, Rocha LAO, Das Neves Gomes M, Dos Santos ED, Isoldi LA. (2015). Constructal design applied to the study of the geometry and submergence of an oscillating water column. International Journal of Heat and Technology 33(2): 31-38. https://doi.org/10.18280/ijht.330205